

## Numerical simulation of shaking table test on concrete gravity dam using plastic damage model

B. Phansri<sup>1</sup>, S. Charoenwongmit<sup>1</sup>, P. Warnitchai<sup>1</sup>, D.H. Shin<sup>2</sup> and K.H. Park<sup>1\*</sup>

<sup>1</sup>*School of Engineering & Technology, Asian Institute of Technology, P.O. Box 4, Klong Luang, Pathumthani 12120, Thailand*

<sup>2</sup>*Head Researcher, Korea Water Resources Corporation, Daejeon, Korea*

*(Received November 25, 2009, Accepted July 30, 2010)*

**Abstract.** The shaking table tests were conducted on two small-scale models (Model 1 and Model 2) to examine the earthquake-induced damage of a concrete gravity dam, which has been planned for the construction with the recommendation of the peak ground acceleration of the maximum credible earthquake of 0.42 g. This study deals with the numerical simulation of shaking table tests for two small-scale dam models. The plastic damage constitutive model is used to simulate the crack/damage behavior of the bentonite-concrete mixture material. The numerical results of the maximum failure acceleration and the crack/damage propagation are compared with experimental results. Numerical results of Model 1 showed similar crack/damage propagation pattern with experimental results, while for Model 2 the similar pattern was obtained by considering the modulus of elasticity of the first and second natural frequencies. The crack/damage initiated at the changing point in the downstream side and then propagated toward the upstream side. Crack/damage accumulation occurred in the neck area at acceleration amplitudes of around 0.55 g~0.60 g and 0.65 g~0.675 g for Model 1 and Model 2, respectively.

**Keywords:** numerical simulation; concrete gravity dam; shaking table test; plastic damage model; earthquake.

---

### 1. Introduction

The construction of new concrete gravity dams has been planned in Southeast Asia. In the construction of dams in the northern Thailand and Myanmar, the seismic loading is needed to be seriously considered because the previous records show some strong earthquake occurrence (Natalaya and Shresta 1990, Myint *et al.* 2008).

Although no complete failure has been reported, some concrete dams have been severely damaged due to the strong ground motion, for example Koyna Dam, India, 1967; Hsingfengkiang Dam, China, 1962; Sefid Rud Dam, Iran, 1990; and Pacoima Dam, California, 1971 and 1994. While the safety evaluation of concrete dams is usually conducted using a linear elastic model based on an allowable maximum tensile stress, the strong earthquake ground motion can produce tensile stress exceeding the tensile strength of the mass concrete (Wieland 2003, Wieland *et al.* 2003). Then cracking or damage will occur in the dam due to tensile stress. Consequently, nonlinear procedures

---

\*Corresponding author, Ph.D., E-mail: [khpark@ait.ac.th](mailto:khpark@ait.ac.th)

are required to examine the earthquake-induced damage of concrete gravity dams.

A number of experimental shaking table tests had been conducted using the small-scale models to examine earthquake-induced damage of concrete dams (Bakhtin and Dumenko 1979, Niwa and Clough 1980, Donlon 1989, Lin *et al.* 1993, Zadnik and Paskalov 1992, Zadnik 1994, Ghobarah and Ghaemian 1998, Tinawi *et al.* 2000, Li *et al.* 2005, Ghaemmaghami and Ghaemian 2008). The difficulties of small-scale model tests are mostly in the development of model material based on similitude requirements, the availability of suitable equipment for testing, and simulating of reservoir and foundation effects. Although small-scale model tests present difficult issues, they have shown that cracking initiates near neck region or the base of model, and then propagates from one side to the other.

On the other hand, numerical analyses had been conducted by using the nonlinear modeling of mass concrete: the discrete crack approach and fracture mechanics (Ayari and Saouma 1990, Feltrin *et al.* 1990), the smeared crack approach (Leger and Leclerc 1996, Calayir and Karaton 2005b), the continuum damage mechanics approach (Calayir and Karaton 2005a), and the plastic damage approach (Lee and Fenves 1998).

A few combined laboratory and numerical modeling studies have been conducted to compare experimental results with numerical results and assess nonlinear models for model material. Ghobarah and Ghaemian (1998) carried out the shaking table test for Pine Flat dam model and compared the maximum principal tensile stress with two-dimensional finite element analysis. Tinawi *et al.* (2000) conducted shaking table tests on four 3.4-m-high concrete dam models to study their dynamic cracking and sliding responses, and compared experimental results with finite element simulation using a smeared crack model based on nonlinear fracture mechanics approach. Li *et al.* (2005) performed the shaking table test for the Three Gorges dam model and compared the results of dynamic magnification factor and maximum dynamic tensile stress with finite element analysis. Ghaemmaghami and Ghaemian (2008) conducted an experimental study of a 1:30 scaled model of the highest monolith of Sefid Rud concrete buttress dam, and compared the crack patterns. The bentonite-based concrete model was described using smeared crack and continuum damage mechanics models. It can be noted from the literature that the use of the plastic damage approach for the bentonite-concrete mixture material, used for small-scale concrete dam models in the shaking table test, has not been adequately addressed.

This study deals with the numerical simulation of shaking table tests for typical concrete gravity dam models using the plastic damage approach. Following the construction plan of a concrete gravity dam (the peak ground acceleration of the maximum credible earthquake in the dam site is recommended as 0.42 g), shaking table tests were conducted on two 1:100 scale models. The numerical simulation of the shaking table tests on small-scale models is performed using the general purpose finite element software ABAQUS (2004). The plane stress analysis is conducted with the assumption of fixed boundary condition at the base. The mechanical behavior of the bentonite-concrete mixture material is described using the plastic damage constitutive model available in the ABAQUS. The parameter values for the plastic damage model are obtained from tensile tests. The numerical results of the maximum failure acceleration and the crack/damage propagation are compared with the experimental results.

It should be noted that the reservoir and foundation effects are neglected due to the experimental limitations. While the tests conducted under the period action of horizontal sinusoidal loading, the results of such tests can be useful to assess numerical models.

## 2. Shaking table test

For the completeness of this study, this section provides brief description on the shaking table tests for two small-scale models. By considering the size of the shaking table (1.2 m × 1.0 m) and the prototype dam, the length scale was set to be 1:100. The properties of model were estimated from those of the prototype dam to match the similitude requirement. Following the estimation of the properties of model, the bentonite-concrete mixture was developed to reduce the corresponding strengths and Young's modulus. The trial mix was separated into two phases in order to find the suitable mixture properties. In the first phase, seven mixtures were proportioned with zero (control mixture), 10, 15, 20, 25, 30 and 45% bentonite by mass of cement plus bentonite. Cement, bentonite and aggregates were obtained from local commercial suppliers. The mixture with 35~40% bentonite gave good results to match the requirements. Based on these results, the second concrete mixture proportions were prepared to construct two small-scale models. Three batches were mixed in each model and nine standard 10 cm × 20 cm cylinders were collected from each batch to identify the physical properties and the stress-displacement curves from tensile tests.

The shaking table test program consisted of two phases using a sinusoidal excitation: (1) resonance test and (2) ambient test. First, the resonance test was conducted to determine the resonant frequency. The model response was recorded at even frequencies from 2 to 30 Hz with a constant input acceleration of 0.05 g. Second, the ambient test was conducted to investigate the maximum failure acceleration and the crack/damage propagation. The models were shaken up to the failure, with the frequencies of 14 Hz for Model 1 and 28 Hz for Model 2, by increasing the acceleration amplitude from 0.05 g to failure. In each step, the acceleration amplitude of 0.0125 g was increased and held 5 seconds.

The results showed that the maximum amplitude accelerations at the base were 0.55 g~0.60 g and 0.625 g for Model 1 and Model 2 respectively, which are higher than the recommended peak ground acceleration of the maximum credible earthquake of 0.42 g. Although the different resonant

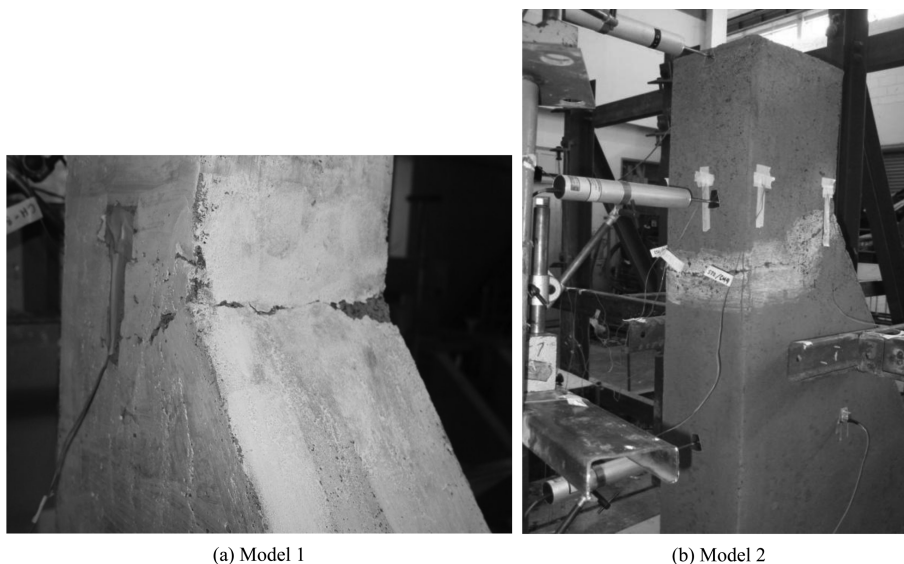


Fig. 1 Crack/damage propagation

frequencies, 14 Hz for Model 1 and 28 Hz for Model 2, were applied, the crack patterns were very similar each other. The crack initiated at the slope changing point in the downstream face and then propagated around the neck area of model, as shown in Fig. 1.

### 3. Numerical simulation

#### 3.1 Finite element model

For the analysis, 4-noded bilinear, reduced integration element, CPSR, is used. The modeling mesh using 819 nodes and 760 elements is shown in Fig. 2. The fixed boundary condition at the base is assumed.

#### 3.2 Material model and properties

The material properties for target and actual models are summarized in Table 1. The bentonite-concrete mixture material is used to reduce the strengths and Young's modulus and match the similitude requirements. While the value of ultimate tensile strength is close to the target value, the values of ultimate tensile strain and the modulus of elasticity are different. For the crack/damage behavior of the bentonite-concrete mixture material, the damaged plasticity constitutive model, available in ABAQUS and based on the models proposed by Lubliner *et al.* (1989) and also Lee and Fenves (1998), is used in this study.

The damaged plasticity model requires the stress-strain behavior of materials under uniaxial compression and tension tests to determine the material properties, for example the modulus of

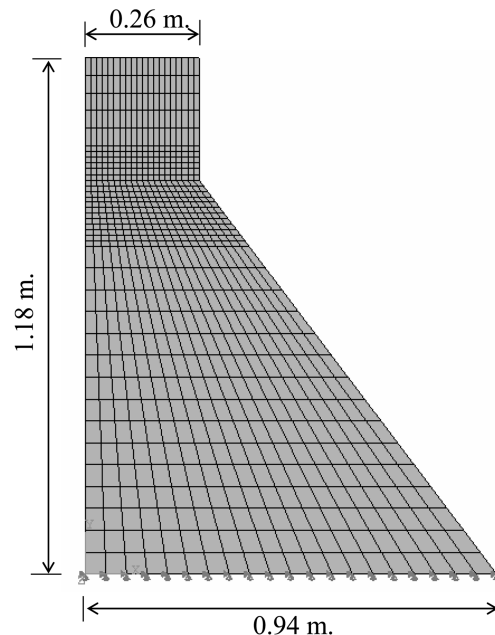


Fig. 2 Modeling mesh

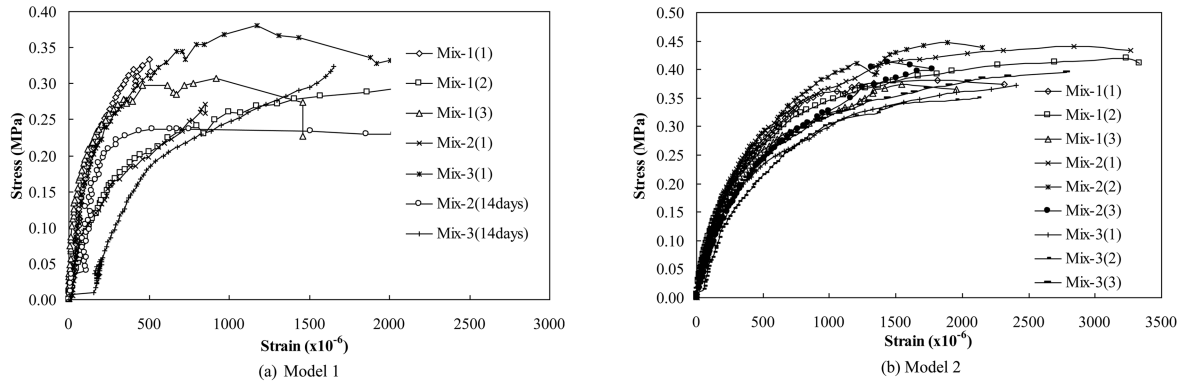


Fig. 3 Stress-strain curves from compressive tests

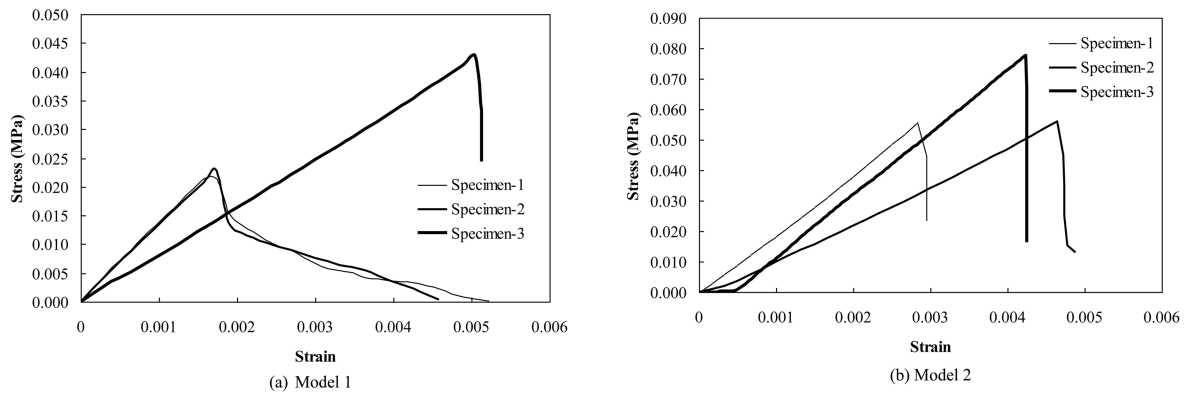


Fig. 4 Stress-strain curves from tensile tests

elasticity, compressive strength and tensile strength. Nine standard  $10\text{ cm} \times 20\text{ cm}$  cylinders in each test were collected to identify the physical properties after 28 days casting. Fig. 3 shows the stress-strain curves of all compression tests for nine cylinders. From Fig. 3, the average values of ultimate compressive strength and strain were obtained. From the stress-strain curve of the direct tensile test (Fig. 4), the ultimate tensile strength and the modulus of elasticity were obtained. In Fig. 4, large variation in the values of tensile strength, tensile strain at the peak strength and the modulus of elasticity can be seen: the peak tensile strength of 0.02~0.08 MPa, the corresponding strain of 0.0015~0.005, and the modulus of elasticity of 13.1~14.2 MPa. Moreover, the material of Model 2 is more brittle than that of Model 1. Model 1 shows the behavior between softening-plastic and brittle, while in Model 2 the strength suddenly drops after the peak value. The modulus of elasticity obtained from the compressive tests is 65~136 times higher than that obtained from the tensile tests. In this study, the modulus of elasticity is taken from the tensile tests because the crack/damage occurs when the tensile stress is over the strength. The average material properties obtained from the stress-strain curves are used in this study (Table 1).

Of particular interest is the tensile behavior of the bentonite-concrete mixture material. In the damaged plasticity model available in ABAQUS (2004), the tensile behavior of material is defined by tension stiffening and tension damage. Based on the stress-strain curve of uniaxial tension (Fig. 4), the tensile stress-crack displacement curve, represented as tension stiffening, is obtained

Table 1 Material properties used in the analysis

Physical property	Unit	Target value	Actual model mix at 28 days	
			Model 1	Model 2
Ultimate compressive strength, $f'_c$	MPa	0.1~0.15	0.317	0.399
Ultimate tensile strength, $f_t$	MPa	0.025		
- Direct tensile			0.029	0.054
- Splitting tensile			0.0135	0.0103
Young's modulus, $E$	MPa	182		
- $E_c$ : Compressive test			1,797.65	905.82
- $E_t$ : Tensile test			13.15	14.16
Mass density, $\rho$	kg/m <sup>3</sup>	2,400	1,907.44	1,936.87
Ultimate compressive strain, $\epsilon_c$	-	0.003	0.00139	0.00262
Ultimate tensile strain, $\epsilon_t$	-	0.00012	0.00495	0.00429
Poisson ratio	-	-	0.2026	0.1930

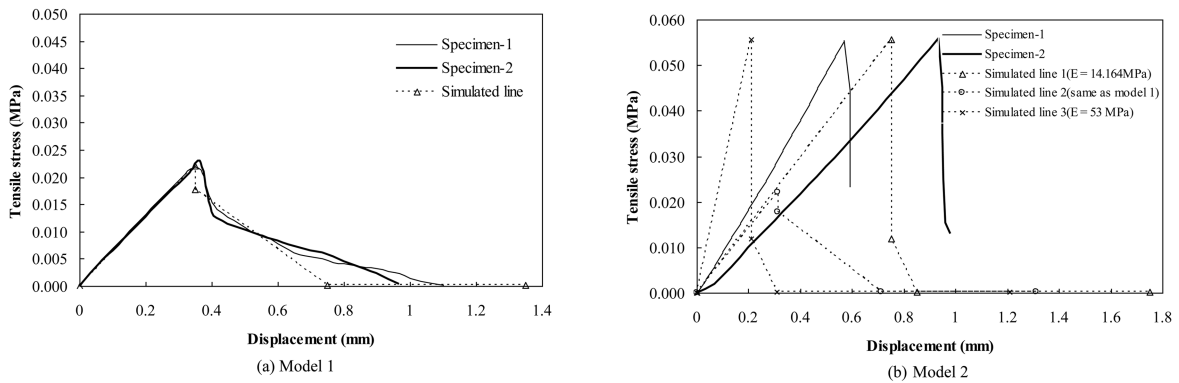


Fig. 5 Tensile stress and displacement

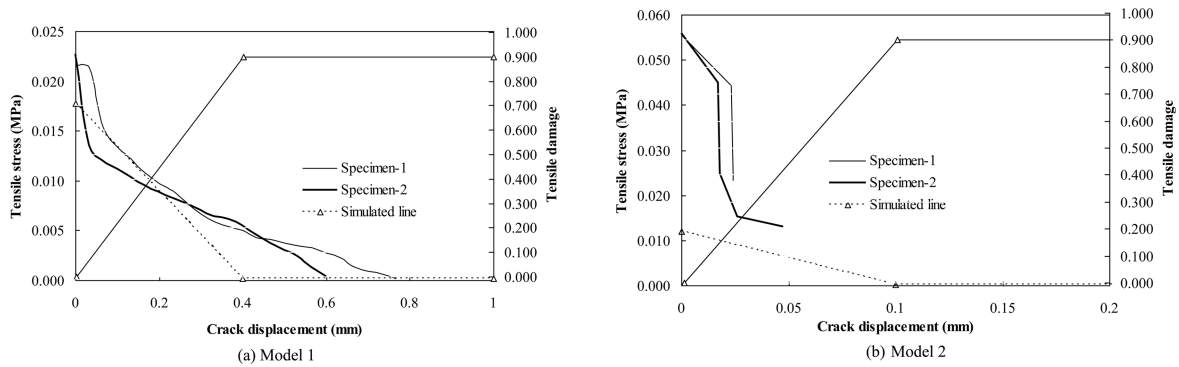


Fig. 6 Tensile properties

from stress-extension displacement (Fig. 5) in the tensile post failure behavior. For the concrete tension damage, the tensile damage as a function of cracking displacement is specified in linear line using value of the maximum damage variable with 0.9, which corresponds to a 90% reduction of the stiffness. The tensile stress-crack displacement and tensile damage-crack displacement curves used in this study are shown in Fig. 6.

Rayleigh stiffness proportional damping is considered in this study. The first or second frequency of the mode in the load direction and damping ratio of 2% are used to determine the  $\beta$  parameter,  $\beta = \xi / \pi f$ , where  $\xi$  = critical damping and  $f$  = natural frequency of selected mode.

### 3.3 Loading conditions

Two loading conditions are considered: gravity loading and sinusoidal acceleration loading. While the gravity loading is applied for the static analysis, the horizontal sinusoidal acceleration loading is applied for the dynamic analysis. In the shaking table test, the crack failure in Model 1 occurred by the horizontal sinusoidal acceleration loading with the frequency of 14 Hz and the base acceleration of 0.55 g~0.60 g, while in Model 2, the crack failure occurred with the frequency of 28 Hz and the base acceleration of 0.625 g. Accordingly, in this study, the base acceleration in Model 1 is varied from 0.50g to 0.60 g with the same frequency of 14 Hz, while for Model 2 the base acceleration of 0.55 g~0.675 g with 28 Hz is considered.

## 4. Results and discussions

### 4.1 Frequency extraction analysis

The frequency extraction analysis is conducted to investigate the fundamental mode of the models. The mode shapes and frequencies for Model 1 and Model 2 are summarized in Table 2. The mode shapes of both models are very similar because of the same shape and similar values of modulus of elasticity.

In the analysis, the first two mode shapes in each model are excited along in the same direction of the acceleration load, while the other modes move out of plane. The frequencies of the first and second modes are 7.55~7.77 Hz and 18.94~19.53 Hz, respectively. The frequency of 14 Hz, used in the shaking table test of Model 1, is in the range of those in the first two modes of the same excited direction, while the frequency of 28 Hz, used in the shaking table test of Model 2, is out of plane.

Since the ratio of the forcing frequency to the natural frequency in harmonic vibration effects the deformation response factor of the model, the natural frequency in the same excited direction is important. For Model 2, the effect of the modulus of elasticity on the natural frequency is investigated. The value of the modulus of elasticity is varied from 14 to 55 MPa, and the results of mode shapes and frequencies are summarized in Table 3. It can be seen from Table 3 that the frequencies in each mode increase with increasing modulus of elasticity. Considering that the ratio of the load frequency to the 2<sup>nd</sup> mode frequency in Model 1 is 0.74, the corresponding modulus of elasticity is estimated by trial and error. The modulus of elasticity of 53 MPa gives the close ratio of 0.74 in Model 2. Table 4 shows the estimated values of damping parameter using the second mode frequency.

Table 2 Mode shape and frequency

Mode	Model 1 ( $E = 13.155$ MPa)		Model 2 ( $E = 14.164$ MPa)	
	Mode shape	Frequency (Hz)	Mode shape	Frequency (Hz)
1		7.5458 <sup>a</sup>		7.7732 <sup>a</sup>
2		18.938 <sup>b</sup>		19.530 <sup>b</sup>
3		21.904		22.552
4		35.037		36.139

Note : ( )<sup>a</sup>, ( )<sup>b</sup> show in the direction of acceleration load

Table 3 Effect of the modulus of elasticity on the natural frequency of Model 2

Modulus of elasticity (MPa)	Frequency (Hz)			
	Mode 1	Mode 2	Mode 3	Mode 4
14.164*	 7.7732	 19.530	 22.552	 36.139
20	9.2405	23.208	26.792	42.943
30	11.321	28.426	32.806	52.592
40	13.074	32.825	37.877	60.727
50	14.619	36.700	42.345	67.894
53**	15.051	37.785	43.596	69.901
55	15.333	38.491	44.411	71.208

Note: ( )\* from the direct tensile test  
( )\*\* from trial & error

#### 4.2 Dynamic analysis

The non-linear responses in this study are shown in terms of the relative displacement and the crack/damage pattern. Figs. 7-10 show the numerical results of relative displacement and propagation of crack/damage for two dam models.

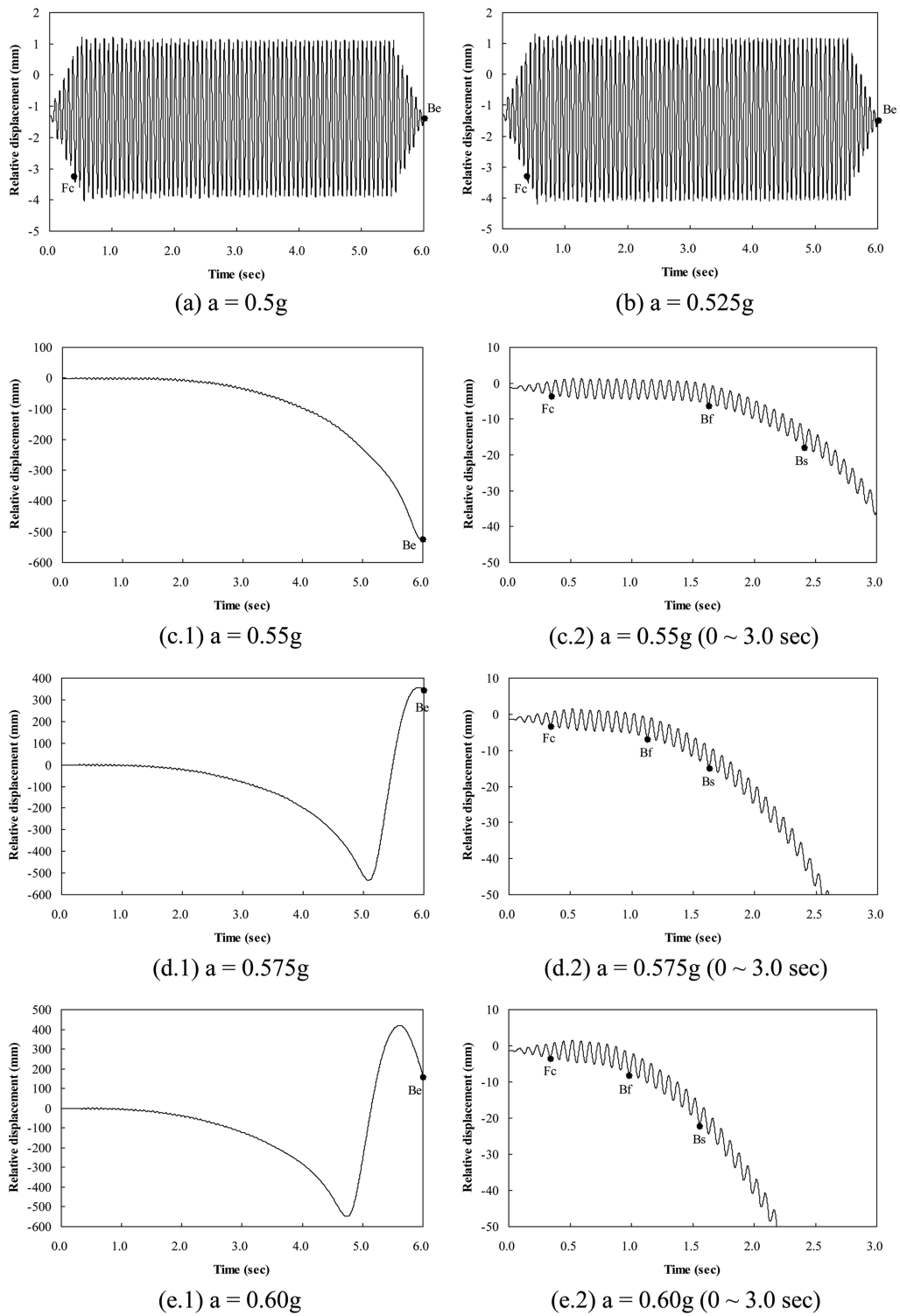


Fig. 7 Relative displacement of Model 1

**4.2.1 Model 1**

The relative displacements at the left corner of the crest of the dam model relative to the base motion (base acceleration of 0.50~0.60 g) are shown in Fig. 7. In figures, points Fc, Bf, Bs and Be indicate the first crack, the crack propagation, the propagated crack around neck area and the crack at the end of motion, respectively.

In Fig. 7, the relative displacement subjected to the base accelerations of 0.50 g and 0.525 g are oscillated until the end of motion. The maximum relative displacements range 1.22~1.33 mm toward downstream side and 4.05~4.21 mm toward upstream side, respectively. The relative displacements increase greatly for the base acceleration of 0.55 g~0.60 g. This indicates the crack failure/damage of the model.

In this study, the tensile damage propagation is investigated using the Damaget parameter. The extents of damage are specified by the percentage ratio of the damage area to the total area, ranging from 0 (undamaged) to 1 (fully damaged). The propagation of crack/damage is shown in Fig. 8.

In Fig. 8, for the base acceleration of 0.50 g~0.525 g, the minor tensile damage is shown in the

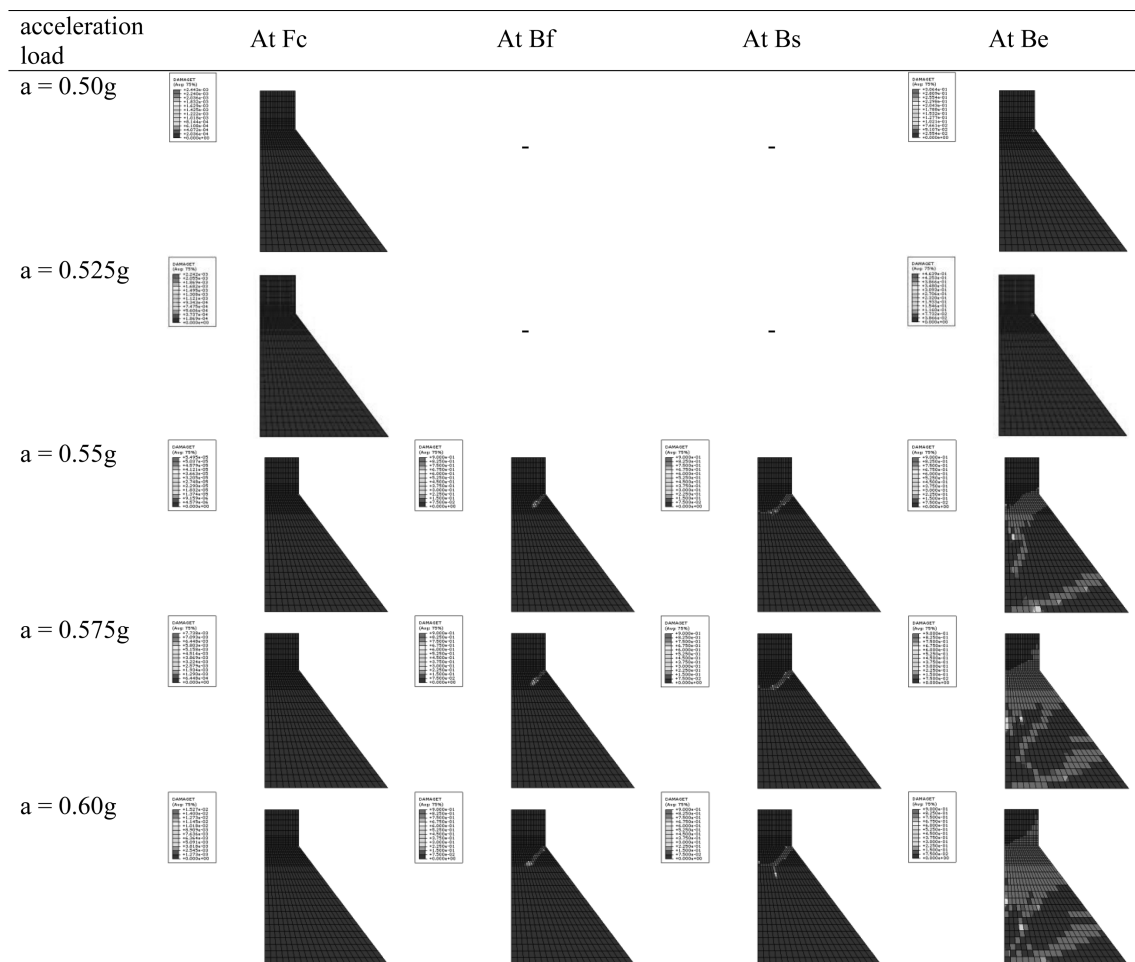


Fig. 8 Propagation of crack/damage of Model 1

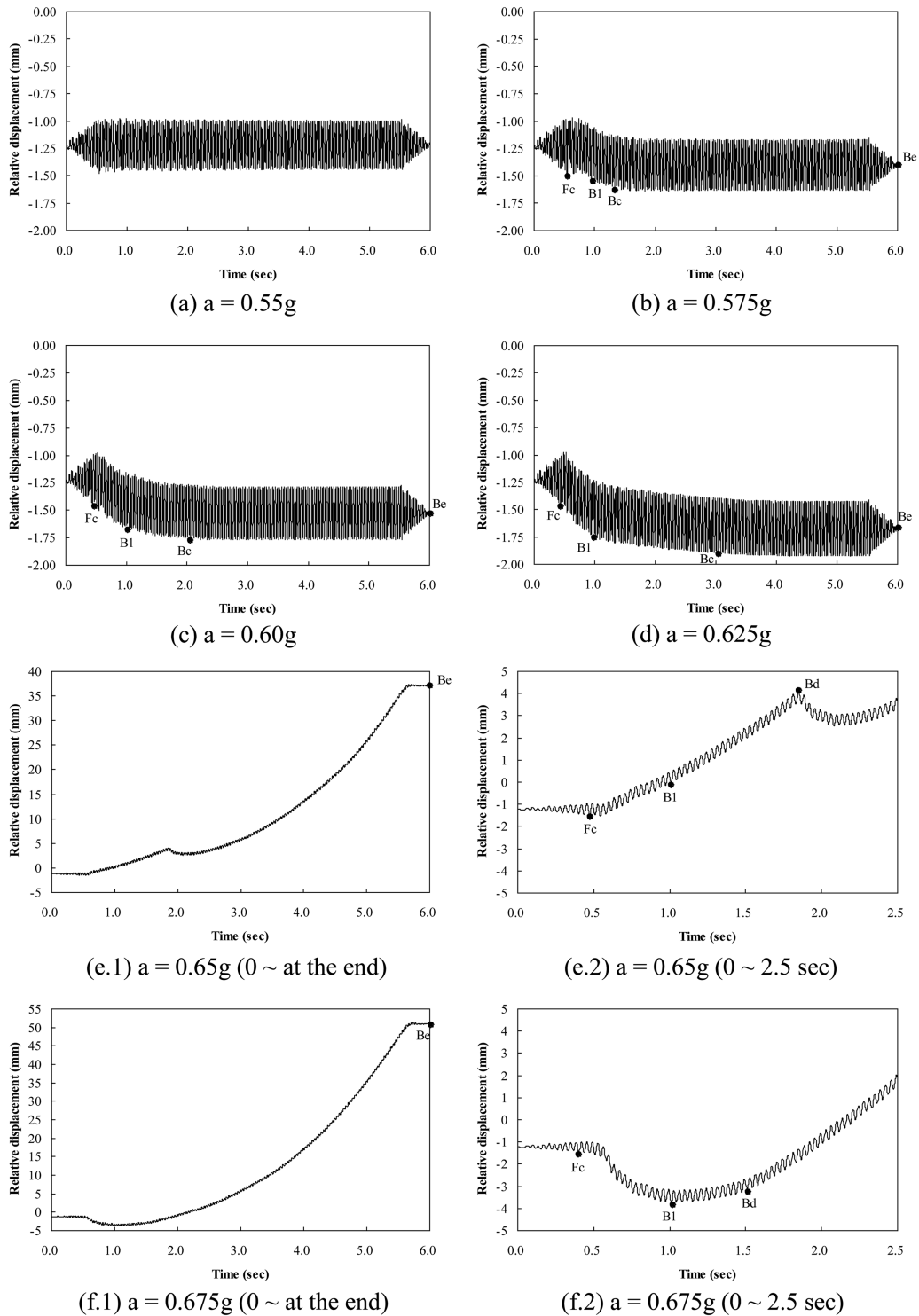


Fig. 9 Relative displacement of Model 2 ( $E = 14.164$  MPa)

slope changing point in the downstream side. However, for the base acceleration of 0.55 g~0.60 g, the crack/damage propagation is obviously seen in the neck area. The damage is initiated at the slope changing point in the downstream face and then propagated toward the upstream face.

Considering the experimental results that the crack/damage initiated at the slope changing point and then propagated from the downstream side to the upstream side, numerical results of crack/damage propagation are in good agreement with experimental results.

**4.2.2 Model 2**

The relative displacement and the propagation of crack/damage for Model 2 are shown in Figs. 9 and 10 for the base acceleration of 0.55 g~0.675 g. In figures, points Fc, B1, Bc, Bd and Be indicate the first crack, the crack at 1.0 sec, the crack at the initial constant relative displacement, the crack at the changed slope of the relative displacement and the crack at the end of motion, respectively.

The relative displacement subjected to the base acceleration of 0.55 g is oscillated until the end of motion. The ranges of maximum relative displacement in the upstream side are 0.975~1.486 mm.

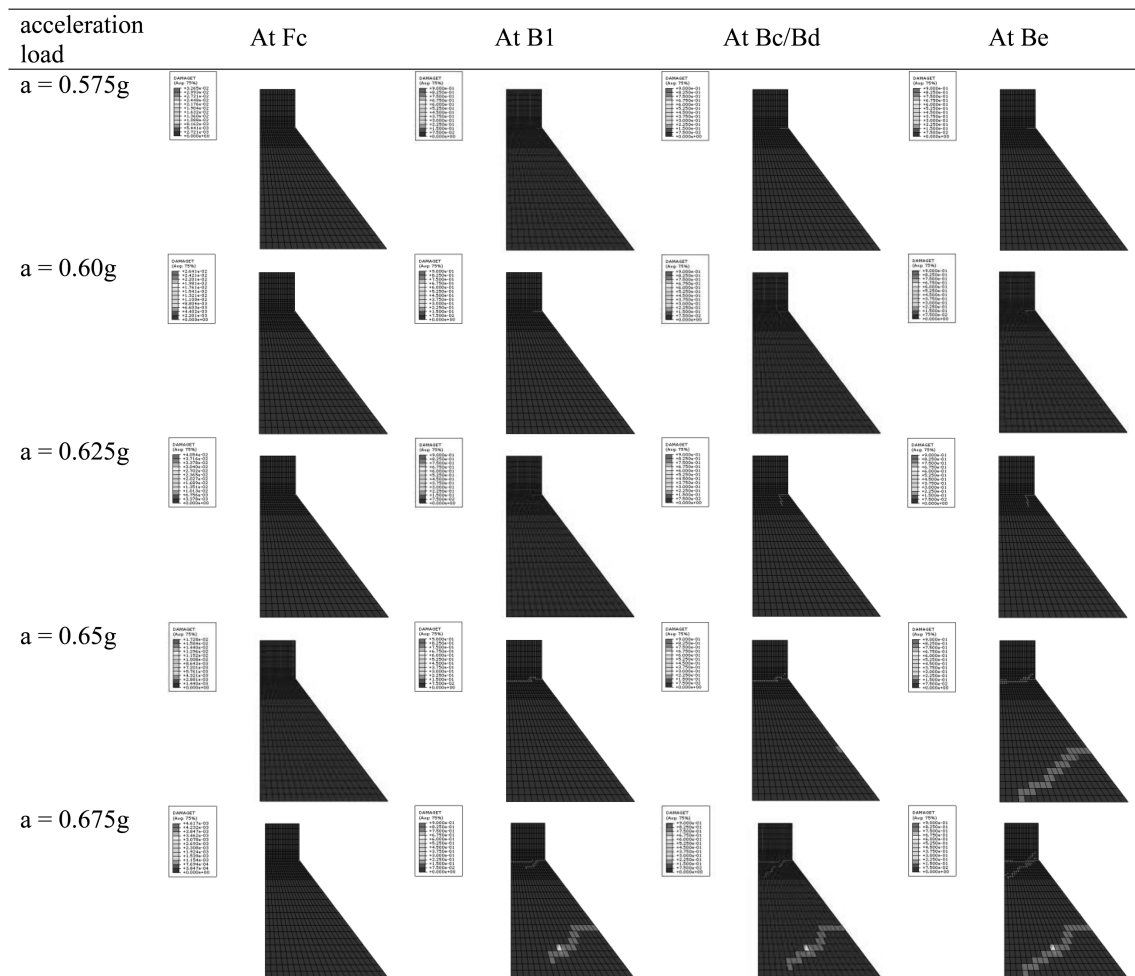


Fig. 10 Propagation of crack/damage of Model 2 ( $E = 14.164 \text{ MPa}$ )

Table 4 The damping parameter used in the analysis

Model	Modulus of elasticity (MPa)	2D analysis	
		Frequency (Hz)	$\beta$ parameter
1	13.155	18.938	0.0003362
2	14.164	19.530	0.0003259
	53.0	37.785	0.001685

Note:  $\beta = \xi/\pi f$ , where  $\xi$  = critical damping,  $f$  = natural frequency of selected mode

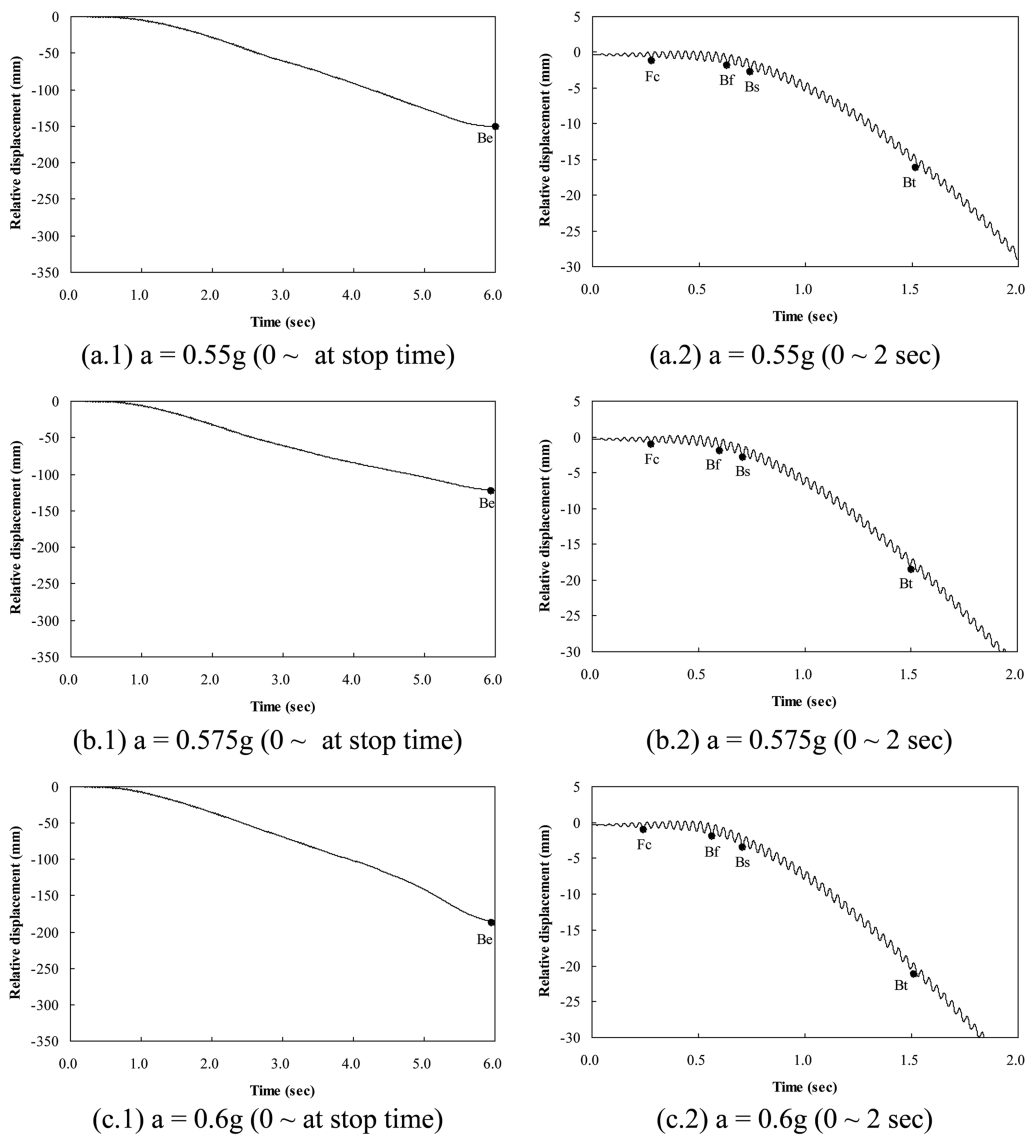


Fig. 11 Relative displacement of Model 2 ( $E = 53$  MPa)

For the base acceleration of 0.575 g~0.625 g, the relative displacement is oscillated in initial few seconds. After the first crack (Fc), the relative displacements increase in upstream direction till around 1.3~3.0 sec and then oscillate until the end of motion. For the base acceleration of 0.65 g~0.675 g, the relative displacements increase in the downstream direction until the end of motion.

For the base acceleration of 0.575 g~0.625 g, the crack/damage is initiated at the slope changing point in the downstream face (Fig. 10). However, for the base acceleration of 0.65 g~0.675 g, another crack/damage appears at the one-third height of the downstream face and propagates toward the bottom of the upstream side.

It is noted that, in the shaking table test of Model 2, the crack/damage initiated at the slope changing point and propagated from the downstream side to the upstream side. While the maximum failure acceleration of 0.65 g~0.675 g is similar to the experimental result, numerical results show the different crack/damage propagation pattern.

### 4.3 Effect of the modulus of elasticity

For Model 2 the dynamic response is investigated by varying the modulus of elasticity with 30 MPa, 40 MPa and 53 MPa. Those values of the modulus of elasticity are considered based on the first two modes in Table 3. It should be noted that these values are in the range of the values obtained from the tensile test ( $E_t = 14$  MPa) and the compressive test ( $E_c = 906$  MPa).

The relative displacements for the base acceleration of 0.55 g~0.6 g, using  $E = 53$  MPa, are shown in Fig. 11. In figures, points Fc, Bf, Bs, Bt and Be indicate the first crack, the crack propagation, the propagated crack around neck area, the crack at 1.4~1.5 sec and the crack at the end of motion, respectively.

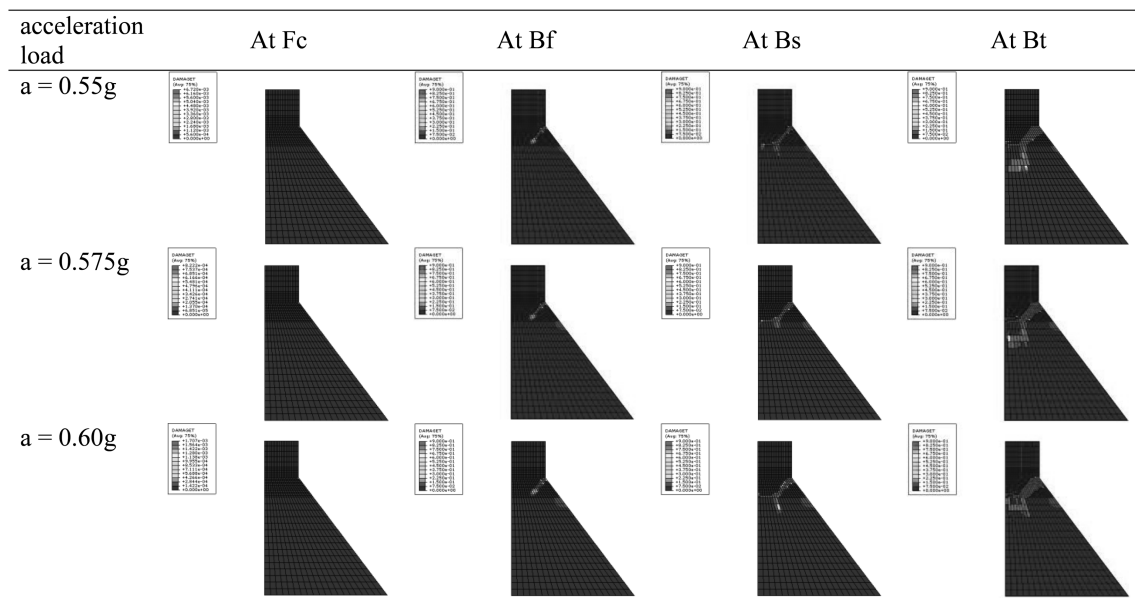


Fig. 12 Propagation of crack/damage of Model 2 ( $E = 53$  MPa)

The results of crack/damage propagation are shown in Fig. 12. While the maximum failure acceleration of 0.55 g~0.6 g is different from the experimental result, the crack/damage pattern in the numerical analysis is similar to experimental result. The crack/damage is found obviously in the neck area and propagated toward the downstream side. Fig. 13 shows the comparison of crack/damage propagation between numerical simulation and experimental results.

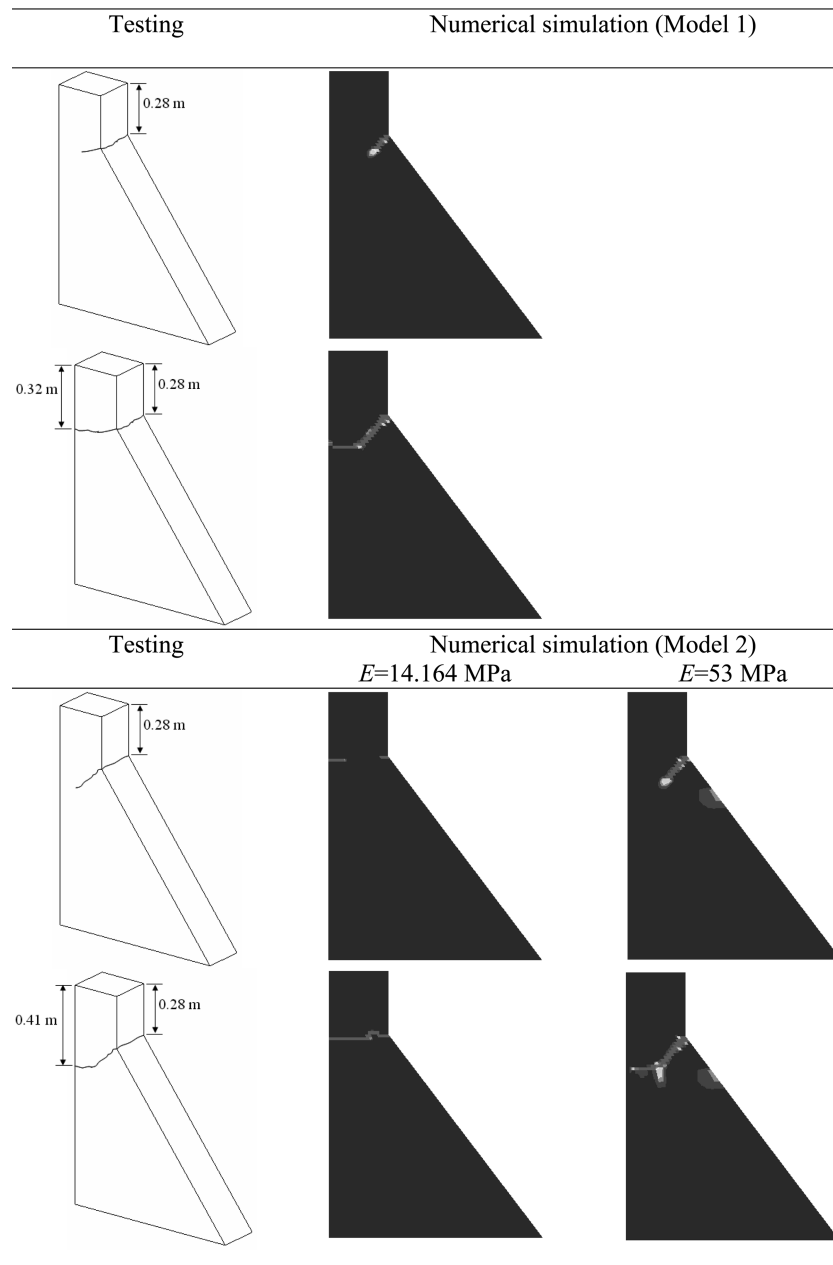


Fig. 13 Comparison of crack/damage propagation patterns

## 5. Conclusions

Numerical simulation of shaking table tests for two small-scale concrete gravity dam models has been performed. The use of plastic damage approach was examined for the crack/damage behavior of bentonite-concrete mixture material.

The following conclusions can be drawn:

(1) In Model 1, for the base acceleration of 0.55 g~0.60 g with the frequency of 14 Hz, the crack/damage is initiated at the slope changing point in the downstream face and then propagated toward the upstream face. The numerical results of the crack/damage propagation pattern are good agreement with experimental results.

(2) In Model 2, the maximum failure acceleration of 0.65 g~0.675 g with the frequency of 28 Hz is similar to the experimental result, the numerical results show the different crack/damage propagation pattern. The crack/damage is initiated at the slope changing point in the downstream face, but other cracks/damages appear at the one-third height of the downstream face and the neck area of upstream side.

(3) For Model 2 the dynamic response is investigated by varying the modulus of elasticity. While the maximum failure acceleration of 0.55 g~0.6 g is lower than the experimental result, the similar crack/damage propagation pattern to experimental result is obtained using  $E = 53$  MPa, which corresponds the similar ratio of the load frequency to the 2<sup>nd</sup> mode frequency in Model 1.

(4) The plastic damage model is used to simulate the crack/damage behavior of the bentonite-concrete mixture material. Overall, the plastic damage mechanics approach was found useful because it is computationally efficient and does not require selection of crack locations a priori.

## References

- ABAQUS Inc. (2004), *ABAQUS 6.5 Documentation*.
- Ayari, M.L. and Saouma, V.E. (1990), "A fracture mechanics approach seismic analysis of concrete gravity dams using discrete cracks", *Eng. Fract. Mech.*, **35**(1-3), 587-598.
- Bakhtin, B.M. and Dumenko, V.I. (1979), "Seismic stability of a concrete gravity dam having a lightweight profile", *Hydrotech. Construct.*, **5**, 445-450.
- Calayir, Y. and Karaton, M. (2005a), "A continuum damage concrete model for earthquake analysis of concrete gravity dam-reservoir systems", *Soil Dyn. Earthq. Eng.*, **25**, 857-869.
- Calayir, Y. and Karaton, M. (2005b), "Seismic fracture analysis of concrete gravity dams including dam-reservoir interaction", *Comput. Struct.*, **83**, 1595-1606.
- Donlon, W.P. (1989), "Experimental investigation of the nonlinear seismic response of concrete gravity dams", Report No. 89-01, Earthquake Engineering Research Laboratory, California Institute of Technology, Pasadena.
- Feltrin, G., Wepf, D. and Bachmann, H. (1990), "Seismic cracking of concrete gravity dams", *Dam Eng.*, **1**(4), 279-289.
- Ghaemmaghami, A.R. and Ghaemian, M. (2008), "Experimental seismic investigation of Sefid-rud concrete buttress dam model on shaking table", *Earthq. Eng. Struct. Dyn.*, **37**, 809-823.
- Ghobarah, A. and Ghaemian, M. (1998), "Experimental study of small scale dam models", *J. Eng. Mech.*, **124**(11), 1241-1248.
- Lee, J. and Fenves, G.L. (1998), "A plastic-damage concrete model for earthquake analysis of dams", *Earthq. Eng. Struct. Dyn.*, **27**, 937-956.
- Leger, P. and Leclerc, M. (1996), "Evaluation of earthquake ground motions to predict cracking response of gravity dams", *Eng. Struct.*, **18**(3), 227-239.
- Li, Q.S., Li, Z.N., Li, G.Q., Meng, J.F. and Tang, J. (2005), "Experimental and numerical seismic investigations

- of the Three Gorges dam”, *Eng. Struct.*, **27**, 501-513.
- Lin, G., Zhou, J. and Fan, C. (1993), “Dynamic model rupture test and safety evaluation of concrete gravity dams”, *Dam Eng.*, **4**(3), 769-786.
- Lubliner, J., Oliver, J., Oller, S. and Onate, E. (1989), “A plastic-damage model for concrete”, *Int. J. Solids Struct.*, **25**(3), 299-326.
- Myint, T., Tun, S.T. and Sew, T.L. (2008), “Current research projects on earthquake and tsunami studies in Myanmar: a progress report”, *Proceedings of the International Symposium on the Restoration Program from Giant Earthquakes and Tsunamis*, Phuket, Thailand.
- Niwa, A. and Clough, R.W. (1980), “Shaking table research on concrete dam models”, Report No. UCB/EERC-80-05, Earthquake Engineering Research Center, College of Engineering, University of California, Berkeley, California.
- Nutalaya, P. and Shrestha. (1990), “Earthquake ground motions and seismic risk in Thailand”, *Proceedings of 1990 Annual Conference*, Engineering Institute of Thailand, Bangkok.
- Tinawi, R., Leger, P., Leclerc, M. and Cipolla, G. (2000), “Seismic safety of gravity dams: from shake table experiments to numerical analyses”, *J. Struct. Eng.*, **126**(4), 518-529.
- Wieland, M. (2003), “Seismic aspects of dams”, General Report, Q.83, *Proceedings of the 21st International Congress on Large Dams*, ICOLD, Montreal, Canada.
- Wieland, M., Brenner, P. and Sommer, P. (2003), “Earthquake resiliency of large concrete dams: damage, repair, and strengthening concepts”, Q.83, *Proceedings of the 21st International Congress on Large Dams*, ICOLD, Montreal, Canada.
- Zadnik, B. and Paskalov, T. (1992), “Dam stability and time-dependent coefficient of friction”, *Proceedings of the 10th World Conference on Earthquake Engineering*, Balkema, Rotterdam, The Netherlands.
- Zadnik, B. (1994), “Motions of rigid unsymmetric bodies and coefficient of friction by earthquake excitations”, *Struct. Eng. Mech.*, **2**(3), 257-267.